IEEE Access
Multidisciplinary | Rapid Review | Open Access Journal

Received January 4, 2020, accepted January 16, 2020, date of publication January 27, 2020, date of current version February 10, 2020.

Digital Object Identifier 10.1109/ACCESS.2020.2969477

A Method for Yaw Error Alignment of Wind Turbine Based on LiDAR

LE ZHANG AND QIANG YANG, (Senior Member, IEEE)
Jiangsu Key Construction Laboratory of IoT Application Technology, Wuxi Taihu University, Wuxi 214064, China

Corresponding author: Le Zhang (75021475@qq.com)

This work was supported in part by the Natural Science Foundation of the Jiangsu Higher Education Institutions of China under Grant 19KJB470033, and in part by the Enterprise Horizontal Project by Wuxi Electronics and Instruments Industry Co., Ltd., under Grant 2019WURD010.

ABSTRACT Yaw control is an important part of the control system of a horizontal shaft wind turbine. After the installation of the wind turbine, the turbulence influence of the wind turbine blades and the azimuth of the wind turbine will cause yaw error which directly affects the economic and the safety of the wind turbine. This article introduces a method for aligning the yaw error of a wind turbine mounted with a LiDAR anemometer, in which the power and the yaw azimuth of the wind turbine, recorded by a SCADA system, are divided into 22 power segments and 12 yaw azimuth sectors respectively. Combining the yaw error angles measured by the LiDAR, a 3D table of yaw error angles is prepared based on the power segments and yaw azimuth sectors of the wind turbine. Using the table of the yaw error angles, the wind turbine yaw error is aligned for capturing the maximum wind energy. According to the analysis of the data measured on-site, the proposed method is found effective in improving the AEP of the aligned wind turbine. Furthermore, taking the alignment of yaw error in a 48.6MW wind farm as an example, the economy and feasibility of the proposed method are analyzed.

INDEX TERMS LiDAR, wind turbine, yaw error alignment.

I. INTRODUCTION

Wind power is the fastest-growing form of renewable energy. The cost of power generation from the wind energy is close to that from conventional energy sources. As of the end of 2018, the world's total capacity of the installed wind power was 593 GW, with an addition of 53.9GW in that year. China's wind energy resources are very rich, totaling installed capacity of 210 GW, with newly added capacity of 21 GW in 2018. China is the country with the highest capacity and growth of wind power installations. As an advanced remote sensing wind measurement technology, the LiDAR (Light Detection and Ranging) has received more and more attention in recent years. In comparison to the conventional mechanical wind vanes and anemometers used in wind turbines, LiDAR has many advantages, such as higher accuracy, flexible installation, measurement of diverse and longer distances. At present, LiDAR has been studied widely in wind power-related research institutions at home and abroad, with successful testing and verification in wind turbines systems [1]–[7].

Apart from the ability to measure the characteristics of wind inflowing towards the rotor of the wind turbine, such as the speed, turbulence and direction, there are several other advantages of employing LiDAR in wind turbines [8]–[11], which are as follows.

(1) The power generation of a wind turbine can be increased and the loads on the structure can be reduced through the yaw error alignment.
(2) The fatigue or extreme load on the towers of a wind turbine can be reduced, and its blades and other components can also be reduced by using a LiDAR measured wind speed feed forward control.
(3) The operating status of wind turbines in a wind farm can be optimized by using a LiDAR coordinated wind field control, where the wake of the wind turbines can be observed.

In provisions (2) and (3) above, usually a high-performance LiDAR is required for measuring the speed, direction, turbulence, shear and wind related other information, which often involves a high investment. As a consequence, most current

The associate editor coordinating the review of this manuscript and approving it for publication was Fabio Massaro.

LiDAR applications in wind power systems are more focused on the yaw error alignment.

At present, two types of approaches are available for aligning yaw error. The first one is for static alignment, where the mean of the difference between the wind directions measured by the LiDAR and the yaw angle measured by wind vane over a long sample period is taken as the fixed yaw error angle. Then, the yaw control system aligns the yaw error by compensating the fixed offset angle. The second approach is for dynamic alignment. In this approach, the wind direction measured by the LiDAR and the yaw angle measured by the wind vane are continuously compared, and the yaw system is dynamically corrected according to the measured values so as to ensure the accuracy of a wind turbine toward the wind direction for capturing the maximum wind energy.

In the approach of static alignment, after aligning the yaw error, the LiDAR can be removed and reused to obtain the maximum economic benefit. However, the fixed yaw error angles cannot reflect the influence of wind speeds and the impact of terrain on the wind vane under different azimuth wind resulted from the variation in the installation location of a wind turbine. Hence, the AEP (annual energy production) from the wind turbine cannot be improved to its maximum limit. Moreover, the continuous cooperation of the LiDAR with the yaw system for aligning the error angle will increase the wear of motors, gears, friction plates and other mechanical components of the yaw system, causing reduction in the service life of this equipment. On the other hand, the approach of dynamic alignment requires every wind turbine to be equipped with a LiDAR for regularly measuring the yaw error, which will increase the cost of the wind turbines and reduce their economic benefits.

On the basis of above, this article presents a method for yaw error alignment of wind turbines based on the nacelle-mounted LiDAR, which can automatically correct the yaw error angle of the wind turbine at different power intervals and also at different yaw azimuths, thus greatly improving the adaptability of yaw error alignment and reducing the dependence of wind turbines on LiDAR. The proposed method is tested and verified in a real wind turbine, and its application economy is analyzed through examples. The article is organized as follows. The principle of using LiDAR to detect yaw error of wind turbines is proposed in section II, followed by the LiDAR based improved method for yaw error alignment in section III. Section IV presents the experimental verification and data analysis. In section V, the economic analysis is performed and finally, the conclusion of the article is drawn in section VI.

II. PRINCIPLE OF LiDAR FOR YAW ERROR ALIGNMENT

The current wind turbines of MW-class mostly adopt an active yaw control strategy. The wind direction and wind speed are taken as inputs to the yaw control system through the wind vane and anemometer respectively. The yaw controller controls the yaw system's action by sending the yaw instructions through logical judgments. Since the anemometer and wind vane are installed in the downwind direction, the measured deviation will inevitably be affected by the turbulence of the blades. The differences in locations of the installed wind turbines will affect their yaw error angles, causing deviation in the yaw control, and subsequently resulting in power loss in the wind turbines. Studies have shown that the power loss (P_{loss}) in a wind turbine is closely related to the square of the cosine of the yaw error angle ($\Delta\phi$)[12], which is expressed by Eq. (1).

$$P_{loss} = P_{rated}(1 - (\cos \Delta\varphi)^2) \tag{1}$$

where P_{rated} represents the rated power capacity of the wind turbine.

A nacelle-mounted LiDAR system can overcome the above stated disadvantages, as it is able to measure the undisturbed inflow over the entire rotor area. Since the beam of LiDAR is located in front of the rotor, the LiDAR can accurately measure the speed and direction of the wind without being affected by the turbulence of the rotor. The LiDAR is fixed on the nacelle of the wind turbine and it rotates synchronously with the yaw of the nacelle. The angle between the axial direction of the nacelle and the direction of the incoming wind measured by the LiDAR can be considered as the error of the yaw control. The measured wind speed along the direction of the laser beam is deduced as expressed by Eq. (2) [13].

$$V_{losi} = \frac{x_i}{f_i}u_i + \frac{y_i}{f_i}v_i + \frac{z_i}{f_i}w_i \tag{2}$$

where V_{losi} represents the measured wind speed along the direction of the i-th laser beam, which is a projection of the wind vector $[u_i\ v_i\ w_i]$ on the direction of the laser beam focusing on the point $[x_i\ y_i\ z_i]$ normalized with the length f_i of that laser beam.

For aligning the yaw error of the wind turbine, the LiDAR requires only the component of the wind speed along the horizontal rotation plane of the yaw, while the vertical component of the wind speed can be ignored. Hence, assuming that the incoming wind has no vertical share, Eq. (2) can be simplified as expressed by Eq. (3).

$$\begin{bmatrix} v_{los,1} \\ \vdots \\ v_{los,n} \end{bmatrix} = \begin{bmatrix} \frac{x}{f_1} & \frac{y_1}{f_1} \\ \vdots & \vdots \\ \frac{x}{f_n} & \frac{y_n}{f_n} \end{bmatrix} \begin{bmatrix} u \\ v \end{bmatrix} \tag{3}$$

Taking two beams of the LiDAR as shown in Figure 1 as an example, the matrix in Eq. (3) can be transformed into a second-order matrix as expressed by Eq. (4), where U and V represent respectively, the horizontal and vertical components of the wind speed at the focal position of the laser beam on the yaw rotation plane. In Eqs. (5) and (6), α represents the angle between the laser beam direction and the LiDAR axial direction.

$$\begin{bmatrix} V_{los1} \\ V_{los2} \end{bmatrix} = \begin{bmatrix} \sin\alpha & \cos\alpha \\ -\sin\alpha & \cos\alpha \end{bmatrix} \begin{bmatrix} U \\ V \end{bmatrix} \tag{4}$$

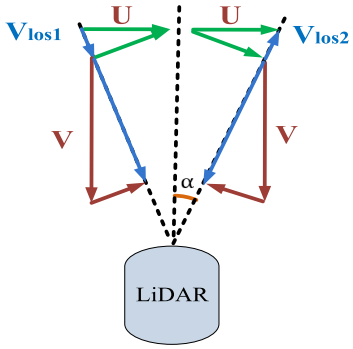

FIGURE 1. Demonstration of the measured wind speeds (V_{los1} and V_{los2}) along two beams of a LiDAR.

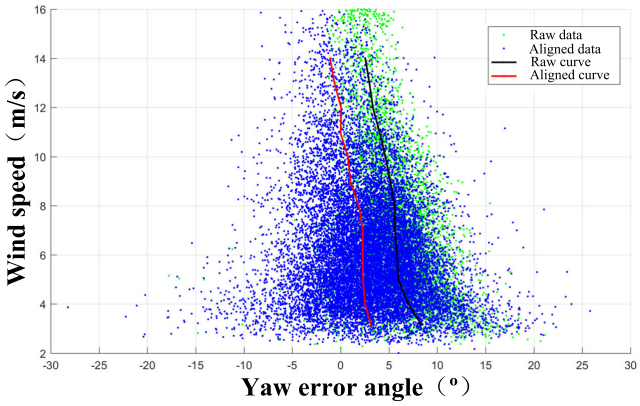

FIGURE 2. Plot of yaw error angle against wind speed.

$$U = \frac{V_{los1} - V_{los2}}{2\sin\alpha} \tag{5}$$

$$V = \frac{V_{los1} + V_{los2}}{2\cos\alpha} \tag{6}$$

$$\Delta\phi = \arctan(\frac{U}{V}) \tag{7}$$

Variables U, V and $\Delta\varphi$ can be worked out from Eq. (4) as shown in Eqs. (5) and (6), respectively. In Eq. (7), $\Delta\varphi$ indicates the angle between the measured wind direction and the LiDAR axial direction. When the LiDAR is installed at the top of the nacelle, $\Delta\varphi$ can be considered as the instantaneous yaw error angle.

III. YAW ERROR ALLIGNMENT METHOD

The average yaw error angle of the wind turbine, $\Delta\phi$, can be calculated by acquiring LiDAR data periodically, particularly at the fully operational wind speed in the 360° yaw azimuth. Figure 2 shows the scatter plot of such data and fitted average curve of the yaw error angle of a wind turbine, where the green and blue colored scatter plots represent the original deviation before and after the yaw error alignment, respectively. The black and red colored continuous curves represent, respectively, the fitted average curves before and after the yaw error alignment. Wind speed interval wise, the sample data of the fitted curves are shown in Table 1, where it can be clearly seen that the aligned yaw error gradually moves to the ideal zero. However, the yaw error angle is still large

TABLE 1. Yaw error angle data and average table.

Wind speed section [m / s]	Average Raw data [°]	Raw data after correction [°]
(4-5)	6.8	2.3
(5-6)	5.6	2.1
(6-7)	5.4	2.1
(7-8)	5.3	1.8
(8-9)	5.1	0.5
(9-10)	4.8	0.2
(10-11)	3.6	-0.5
(11-12)	3.2	-0.8
(12-13)	2.8	-1.2
(13-14)	2.5	-1.5
Total average	4.51	0.5

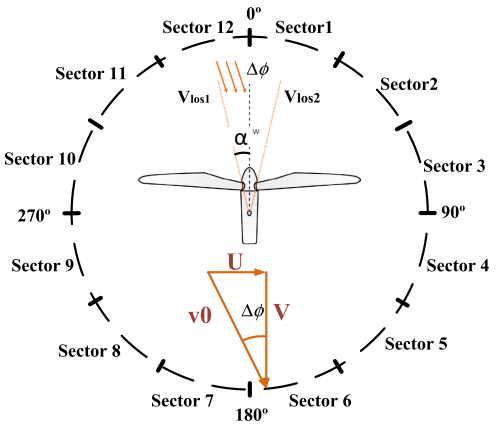

FIGURE 3. Yaw error diagram of LiDAR.

at different intervals of the wind speed, which means that the average value could not accurately compensate in those power sections, resulting to higher power loss there.

Since most wind turbines use variable pitch angle control, the corresponding angles of the blade pitch under different intervals of the wind speed are different, and the impact of the blade turbulence on the wind vane of the yaw azimuth is not exactly the same. Therefore, when the yaw error angle is supplemented, the effects of the output power and the yaw azimuth of the wind turbine must be fully considered.

Based on the above analysis, the wind speed in its entire range is divided into multiple power ranges, each range of 100 kW power. In order to avoid the frequent movement of the yaw system with the change in wind direction, most of the adjustment ranges of the yaw control are kept in $[-15°, +15°]$. The entire yaw range is divided into 12 sectors with 30° in each sector. For maximizing power output, the yaw error of the wind turbine is aligned in different power segments and yaw sectors. Figure 3 shows the schematic diagram of the LiDAR yaw azimuth sector. The zero position assigned to the sector is taken at the yaw azimuth 0° angle. The sector is allocated using the remainder obtained after dividing the yaw angle by 360°.

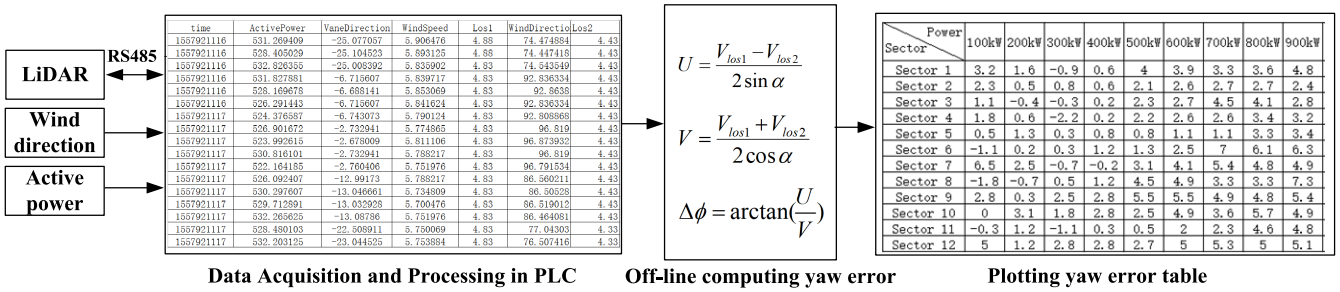

time	ActivePower	VaneDirection	WindSpeed	Los1	WindDirectio	Los2
1557921116	531.269409	-25.077057	5.906476	4.88	74.474884	4.43
1557921116	528.405029	-25.104523	5.893125	4.88	74.447418	4.43
1557921116	532.826355	-25.006392	5.835902	4.83	74.543549	4.43
1557921116	531.827881	-6.715607	5.839717	4.83	92.836334	4.43
1557921116	528.169678	-6.688141	5.853069	4.83	92.8638	4.43
1557921116	526.291443	-6.715607	5.841624	4.83	92.836334	4.43
1557921117	524.376587	-6.743073	5.790124	4.83	92.808868	4.43
1557921117	526.901672	-2.732941	5.774865	4.83	96.819	4.43
1557921117	523.992615	-2.678009	5.811106	4.83	96.873932	4.43
1557921117	530.816101	-2.732941	5.788217	4.83	96.819	4.43
1557921117	522.164185	-2.760406	5.751976	4.83	96.791534	4.43
1557921117	526.092407	-12.99173	5.788217	4.83	86.560211	4.43
1557921117	530.297607	-13.046661	5.734809	4.83	86.50528	4.43
1557921117	529.715591	-13.032928	5.700476	4.83	86.519012	4.43
1557921117	532.265625	-13.08786	5.751976	4.83	86.464081	4.43
1557921117	528.480103	-22.508911	5.750069	4.83	77.04303	4.33
1557921117	532.203125	-23.044525	5.753884	4.83	76.507416	4.33

$$U = \frac{V_{los1} - V_{los2}}{2\sin\alpha}$$

$$V = \frac{V_{los1} + V_{los2}}{2\cos\alpha}$$

$$\Delta\phi = \arctan(\frac{U}{V})$$

Power / Sector	100kW	200kW	300kW	400kW	500kW	600kW	700kW	800kW	900kW
Sector 1	3.2	1.6	-0.9	0.6	4	3.9	3.3	3.6	4.8
Sector 2	2.3	0.5	0.8	0.6	2.1	2.6	2.7	2.7	2.4
Sector 3	1.1	-0.4	-0.3	0.2	2.3	2.7	4.5	4.1	2.8
Sector 4	1.8	0.6	-2.2	0.2	2.2	2.6	2.6	3.4	3.2
Sector 5	0.5	1.3	0.3	0.8	0.8	1.1	1.1	3.3	3.4
Sector 6	-1.1	0.2	0.3	1.2	1.3	2.5	7	6.1	6.3
Sector 7	6.5	2.5	-0.7	-0.2	3.1	4.1	5.4	4.8	4.9
Sector 8	-1.8	-0.7	0.5	1.2	4.5	4.9	3.3	3.3	7.3
Sector 9	2.8	0.3	2.5	2.8	5.5	5.5	4.9	4.8	5.4
Sector 10	0	3.1	1.8	2.8	2.5	4.9	3.6	5.7	4.9
Sector 11	-0.3	1.2	-1.1	0.3	0.5	2	2.3	4.6	4.8
Sector 12	5	1.2	2.8	2.8	2.7	5	5.3	5	5.1

FIGURE 4. Procedure for generating a three-dimensional table of yaw error angles.

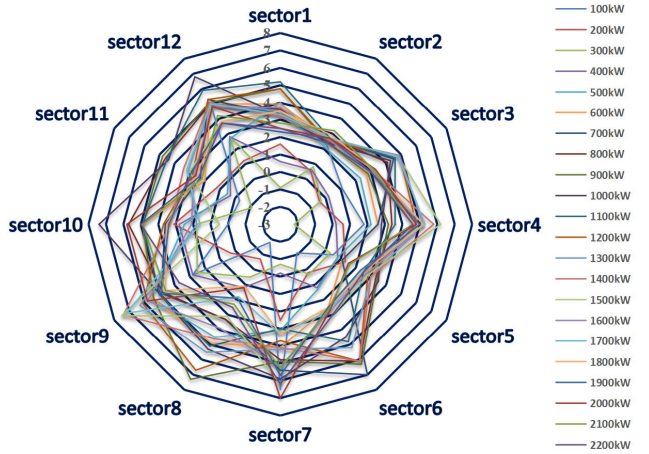

FIGURE 5. Yaw error corresponding to different power segments and yaw azimuth sectors.

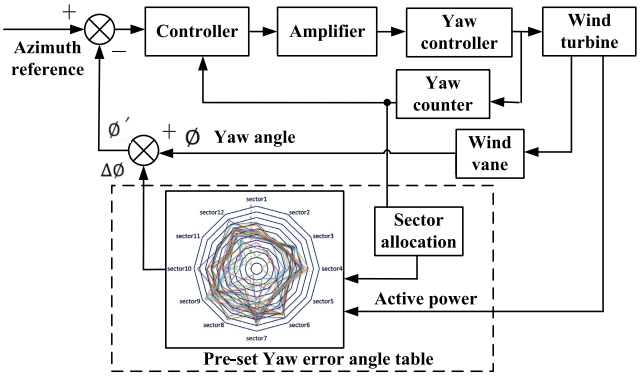

FIGURE 6. Flowchart of Yaw control along with the proposed yaw error alignment model.

TABLE 2. Parameters of the tested wind turbines and LiDAR.

Turbine parameters	Value
Rated power / kW	2200
Generator rated speed / (r / min)	1800
Annual average wind speed / (m / s)	5.5
Tower height / (m)	100
Rotor swept diameter / (m)	121
IEC turbulence coefficient	B
LiDAR parameters	**Value**
Installation position	On nacelle
Laser Beam Type	Continuous
Measuring distance f_i / (m)	80
Numbers of beams	4
Beam horizontal half-angle α / (o)	13
Beam vertical half-angle β / (o)	13

The procedure of generating the three-dimensional table of yaw error angles is shown in Figure 4. The raw data of the wind measured by the LiDAR is transmitted to the main controller PLC of the wind turbine through a communication BUS (such as RS485 interface). The data related to the operation of the wind turbine and wind directions, acquired by the PLC, are sent to the wind field of the SCADA system. Using Eqs. (3) to (7), the yaw error angles table can be prepared and plotted. It should be noted that the plot of the entire table of yaw error angles requires long-term data to satisfy that every yaw azimuth sector and all the operating power segments have enough data, which are huge in size. The off-line computation can avoid the requirement of excessive memory capacity and computing power in the PLC controller of the wind turbine. The resulting datasets of 12 consecutive sector planes are plotted as shown in Figure 5, where the yaw errors in different power segments and the three-dimensional yaw error angle for the entire wind turbine power segment are plotted by continuous lines of different colors.

Finally, the generated table of the yaw error angles is added to the yaw control algorithm of the wind turbine. A flowchart of the yaw control of the wind turbine after the addition of the proposed yaw error alignment method is shown in Figure 6, where the dashed box is the newly added yaw error alignment model, According to the values of the yaw counter, the operating yaw azimuth sectors of the wind turbine are calculated in the sector allocation module, and the current yaw error angle $\Delta\phi$ is obtained according to the corresponding wind turbine output power look-up table. Combine the table as a feedback compensation amount with the yaw angle ϕ to generate an aligned and controlled yaw angle reference ϕ'。

IV. EXPERIMENTAL VERIFICATION AND DATA ANALYSIS

According to the aforementioned method, an experiment was performed in a real wind turbine using LiDAR to verify the validity of the proposed method and to analyze the factors for improving the power generating capacity of wind turbines. The data of the tested wind turbine and the LiDAR are given in Table 2. A 3-months cycle of time period was considered for collecting data from the wind turbine. In this experiment, the AEP was calculated by comparing the increase in power generation after the yaw error alignment with that generated

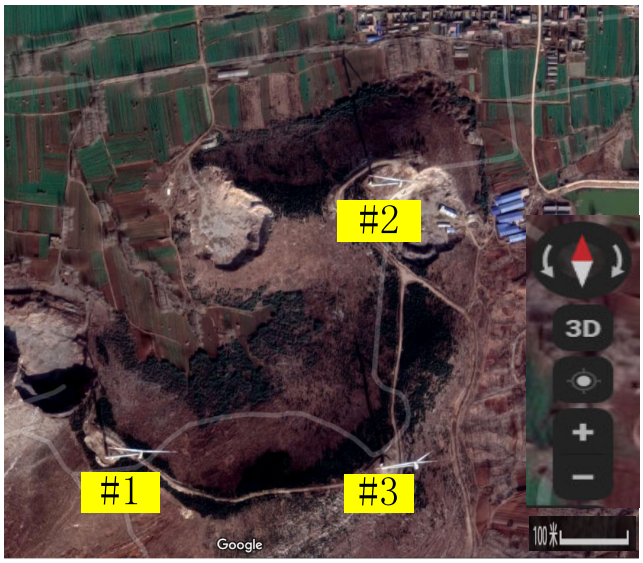

FIGURE 7. Location of the wind turbines used in the experiment.

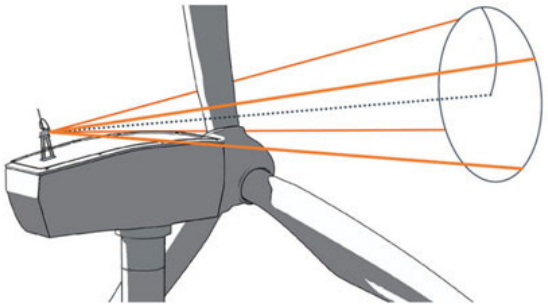

(a) Schematic diagram of the LiDAR beam

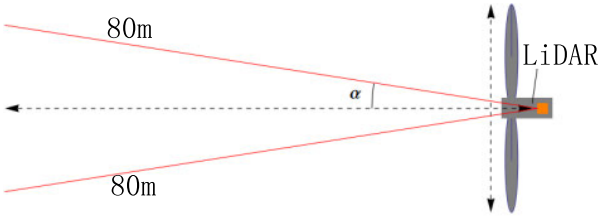

(b) Top view of the wind turbine

FIGURE 8. Schematic diagram of the tested wind turbine with LiDAR.

by adjacent wind turbines in the same period without aligning its yaw error.

The locations of the wind turbines are shown in Figure 7, where #2 was the target turbine with installed LiDAR for yaw error alignment, and #3 was the turbine whose generated power was compared with that of #2. The distance between the installed locations of the two turbines is about 500m.

In order to get accurate measurements, the LiDAR was correctly installed on the wind turbine. Figure 8 showed the position of the LiDAR on the turbine.

For the experiment on the yaw error alignment of the wind turbine, data was collected in the period from August 16, 2018 to October 24, 2018. The LiDAR continuously sampled

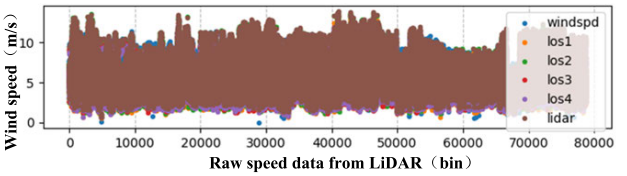

(a)Raw wind speed data measured by LiDAR

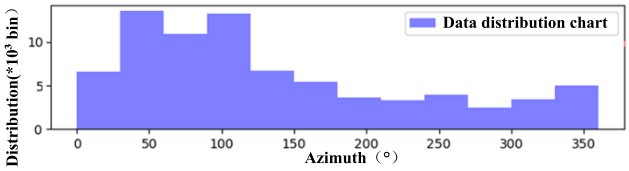

(b)Distribution of the raw data in 360° yaw azimuth sectors

FIGURE 9. Distribution of the measured valid date of wind speed.

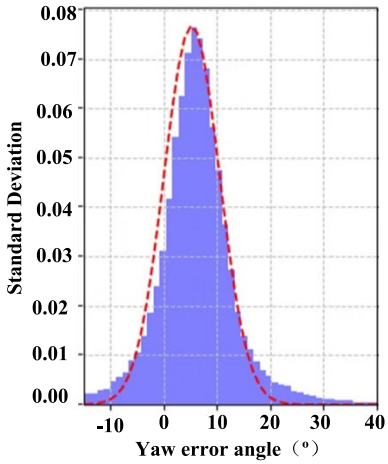

FIGURE 10. Standard deviation of all the data of yaw error angle.

the wind data at 1Hz sampling frequency. Before aligning the yaw error, the raw data of the wind speed, measured by the LiDAR, were required to be cleaned and filtered as follows.

(1) The turbine was operating normally.
(2) The bad points in the process of measurement were eliminated, including invalid measurement points generated by those blades blocking the beam.
(3) Low SNR (signal noise ratio) in data of the wind speed, caused by bad weather (such as rain, snow, and fog), are eliminated.

There were about 79,000 sets of valid data after cleaning and filtering, which are shown in Figure 9. The data of each set represented the average value of the wind speed in 1 minute. There were a relatively large number of collected samples in the entire 0 ∼ 360° yaw azimuth, which guaranteed a high reliability of the data when the three-dimensional yaw error angle was plotted in the later stage.

Figure 10 showed the standard deviation of the yaw error angle calculated from the data of wind speed measured by the LiDAR. The figure did not distinguish the difference between the power band and the yaw azimuth, but showed only the statistical standard deviation of 79,000 sets of data. It can be seen that #2 wind turbine has obvious yaw error angle.

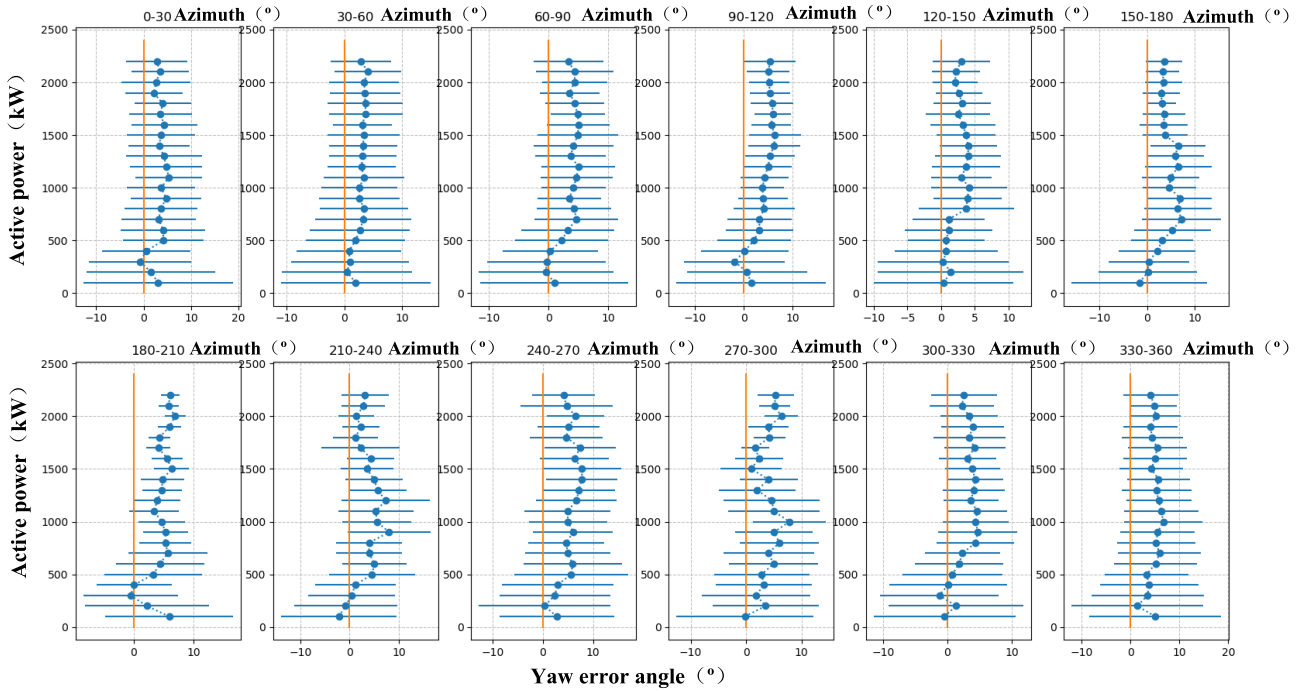

FIGURE 11. Sector-wise plots of yaw error angle.

Before generating the table of yaw error angles required for the yaw control, the data shown in Figure 10 were required to be filtered again by limiting the standard deviation of the yaw error angle within ±15°. Those filtered data were used to generate a three-dimensional table of yaw error angles, applicable for the yaw control based on the yaw angle sectors and power segments. Sector-wise plots of the yaw error angles for all the 12 sectors are shown in Figure 11, where each graph is fitted in a power segment of 100 kW. The orange colored continuous lines represent the position where the yaw error angle is zero, while the blue colored horizontal lines represent the yaw error angles and the blue colored dots represent the average yaw error angle in the current power segment. The yaw error correction table prepared from plots of Figure 11 was embedded in the yaw control system of the wind turbine for yaw error alignment control. The plots of the power curves before and after the yaw error alignment were shown in Figure 12, where Figure 12(a) showed the wind power curve before alignment for the data sets of the period from August 16, 2018 to October 24, 2018, and Figure 12(b) showed the wind power curve for the data sets of the period from October 25, 2018 to March 11, 2019. The blue and red colored dots in Figure 12 represent the power data of wind turbines #2 and #3, respectively, where each dot represented the average value of the data of a period of 10 minutes. Black and green colored curves were the fitted power curves of wind turbines #2 and #3, respectively. The wind speed in the figure 12 were all measured by the conventional anemometers on wind turbine nacelle.

As can be seen from the above power curves of Figure 12, the 2# target wind turbine power curve had been significantly improved after the yaw error alignment, especially in the wind speed region of 6-8m/s. In order to found out the influence of yaw error alignment method on the wind turbine energy production, The AEP of 2# and 3# wind turbines were calculated respectively both before and after yaw error correction based on wind speed frequency distribution of this wind field presented in figure 13 measured by mast.

Considering that the change of wind speed, wind direction, temperature and other external conditions in different periods will affect the power curve measurement. The method of comparing the relative AEP improvement in the different test period (before and after yaw error alignment) was adopted, through this comparison, the incremental error caused by the change of different measurement environment can be eliminated. The AEP comparison before the yaw error alignment was found as $\frac{AEP(\#2)_{\text{before}}}{AEP(\#3)} = 6.78\%$, while it became $\frac{AEP(\#2)_{\text{after}}}{AEP(\#3)} = 8.61\%$ after the yaw error alignment. Hence, it was found that the AEP for the wind turbine with the proposed method was improved by 1.83%. By using the AEP evaluation method, the effect of yaw error alignment on wind turbine energy production and revenue improvement can be truly reflected.

V. ECONOMIC ANALYSIS

The high cost of LiDAR has been one of the key constraints for its large-scale application in wind turbine systems. In order to evaluate the relationship between the improved AEP of a wind turbine obtained upon aligning its yaw error

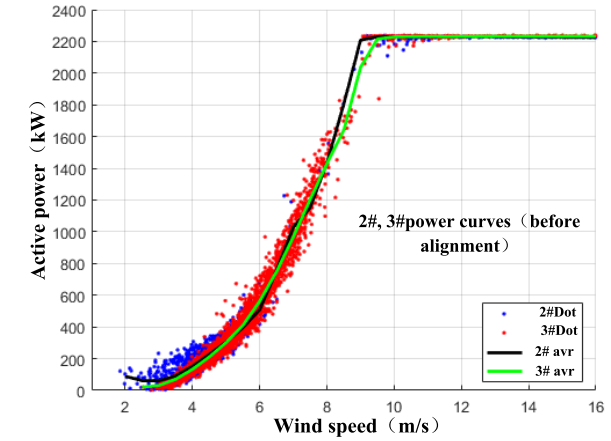

(a) Before yaw error alignment (Data from August 16, 2018 to October 24, 2018

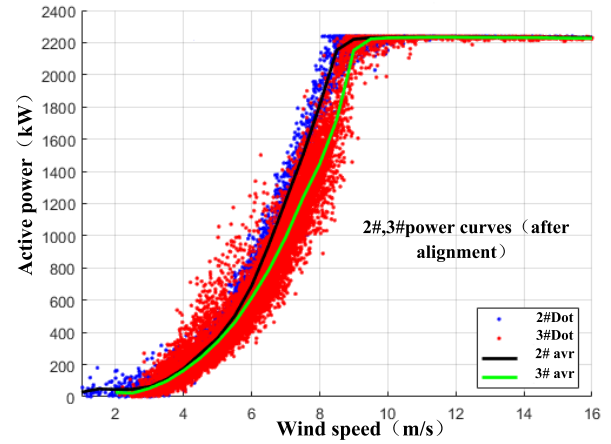

(b) After yaw error alignment (Data from October 25, 2018 to March 11, 2019)

FIGURE 12. Power curves of wind turbines #2 and #3 before and after yaw error alignment.

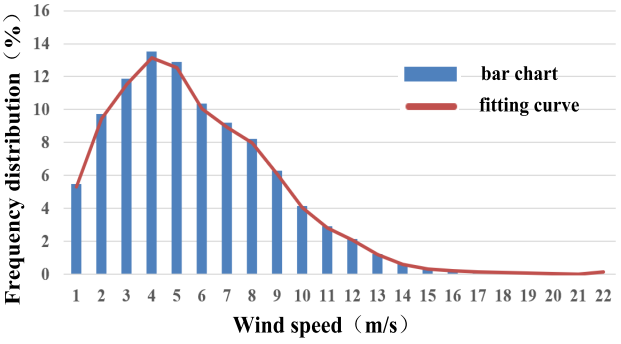

FIGURE 13. Wind speed frequency distribution.

TABLE 3. Detail of the lidar incorporated wind field used in the economic analysis.

Total capacity of the wind field (MW)	48.6
Number of wind turbines (Sets)	22
Capacity of a single wind turbine (kW)	2200
Cost of a LiDAR (RMB)	150,000
On-grid price of electricity (RMB/kWh)	0.5
AEP (Hours):	2500
Duration of data acquisition (Months)	3

TABLE 4. Evaluation of return of investment(ROI) cycle of lidar used in the economic analysis.

AEP promotion rate (%)	Annual profit of one turbine (RMB)	ROI cycle of 5 LiDARs (Year)	ROI cycle of 7 LiDARs (Year)
3.5	96250	1.03	1.02
3	82500	1.09	1.11
2.5	68750	1.17	1.23
2	55000	1.30	1.41
1.5	41250	1.52	1.71
1.0	27500	1.95	2.32

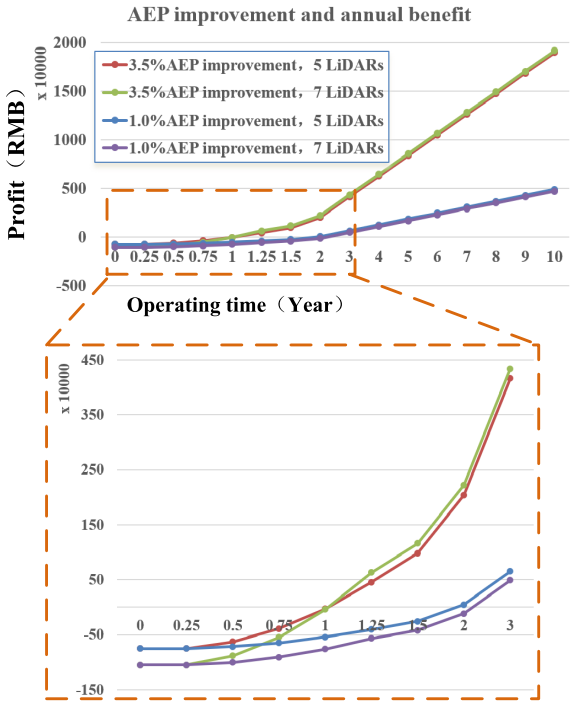

FIGURE 14. Assessment of capital gain under presumed rates of AEP promotion.

and the cost return cycle of the LiDAR investment, the real data from a 48.6MW wind farm were collected, which were presented in Tables 3 and 4. For implementing the wind turbines yaw error alignment, the wind farm uses multiple LiDARs at the same time. After the completion of the alignment in one wind turbine, the LiDAR was removed from it and installed in another wind turbine. The process was continued until alignment in all the wind turbines of the farm was completed. Two schemes for alignment, one using 5 LiDARs and the other using 7 LiDARs at the same time, were compared. The comparison took into account the LiDAR data acquisition time cycle used by the LiDAR, but ignored the time and cost of the LiDAR installation, and LiDAR removal time and commissioning. The focus was only on the period of capital return on LiDAR equipment investment.

According to the results presented in Table 4 with the assumption that the average promotion rate of the AEP lied

in the range from 1% to 3.5%, the time curve of the assessed capital gain was plotted as shown in Figure 14. It was assumed that the average replacement cycle of the wind vane was 10 years, and the yaw error angle of the wind turbine needs to be aligned again when the wind vane was replaced. Hence, the income period in the plot of Figure 14 was also taken as 10 years. It can be seen in Figure 13 that when the average AEP promotion rate of the wind farm reaches 3.5%, the capital invested on LiDAR equipment can be recovered within one year by increasing the amount of power to be generated by the wind turbine, and a cumulative profit of nearly 20 million RMB can be obtained in a life cycle of 10 years. Even if the average AEP promotion rate was only 1%, the capital invested on LiDAR equipment can be recovered within 2 years, and an accumulated profit of nearly 5 million RMB can be made in the 10th year. Moreover, the LiDAR removed from one wind turbine, after aligning it, can be reused in another wind turbine. Accordingly, it can be seen clearly that the proposed yaw error alignment method has good practical and economic values.

VI. CONCLUSION

This article proposes a novel method for yaw error alignment based on LiDAR measured flow direction of the incoming wind. The method could successfully align the yaw error of a wind turbine by using a three-dimensional table of yaw error prepared on the basis of power segments and yaw azimuth sections of the wind turbine.

Through the test and comparison in a specific wind turbine site, it is found that the AEP of the wind turbine could be increased by 1.83% through the proposed method. The experimental results verified that the method could effectively increase power generation of the wind turbine.

The cycle for return of investment by the method is simulated in a 48.6MW wind farm, where two schemes (one using 5 LiDARs and the other using 7 LiDARs) are used for yaw error alignment of the turbines. The simulated results show that, even if the AEP of the yaw error aligned wind turbines is increased by 1%, the wind field can recover the investment made on the LiDAR within 2 years by improving the power to be generated by the wind turbines. It proves that the proposed method has good practicability and profit.

REFERENCES

[1] E. Simley, H. Fürst, F. Haizmann, and D. Schlipf, "Optimizing lidars for wind turbine control applications-results from the iea wind task 32 workshop," *Remote Sens.*, vol. 10, no. 6, p. 863, Jun. 2018.

[2] P. A. Fleming, A. K. Scholbrock, A. Jehu, S. Davoust, E. Osler, A. D. Wright, and A. Clifton, "Field-test results using a nacelle-mounted lidar for improving wind turbine power capture by reducing yaw misalignment," *J. Phys. Conf. Ser.*, vol. 524, Jun. 2014, Art. no. 012002.

[3] D. Held and J. Mann, "Lidar estimation of rotor effective wind speed-an experimental comparison," *Wind Energy Sci.*, vol. 4,no. 3, pp. 421–438, 2019.

[4] A. Peña, C. B. Hasager, S.-E. Gryning, M. Courtney, I. Antoniou, and T. Mikkelsen, "Offshore wind profiling using light detection and ranging measurements," *Wind Energy*, vol. 12, no. 2, pp. 105–124, Mar. 2009.

[5] T. Mikkelsen, N. Angelou, K. Hansen, M. Sjöholm, M. Harris, C. Slinger, P. Hadley, R. Scullion, G. Ellis, and G. Vives, "A spinner-integrated wind lidar for enhanced wind turbine control," *Wind Energy*, vol. 16, no. 4, pp. 625–643, May 2013.

[6] N. Wang, K. E. Johnson, and A. D. Wright, "Comparison of strategies for enhancing energy capture and reducing loads using lidar and feedforward control," *IEEE Trans. Control Syst. Technol.*, vol. 21, no. 4, pp. 1129–1142, Jul. 2013.

[7] E. Dellwik, M. Sjöholm, and J. Mann, "An evaluation of the windeye wind lidar," *DTU Wind Energy*, pp. 1–13, Feb. 2015.

[8] R. Damiani, S. Dana, J. Annoni, P. Fleming, J. Roadman, J. Van Dam, and K. Dykes, "Assessment of wind turbine component loads under yaw-offset conditions," *Wind Energies Sci.*, vol. 3, no. 1, pp. 173–189, Apr. 2018.

[9] H. Dhiman, D. Deb, V. Muresan, and V. Balas, "Wake management in wind farms: An Adaptive control approach," *Energies*, vol. 12, no. 7, p. 1247, Apr. 2019.

[10] M. Bromm, A. Rott, H. Beck, L. Vollmer, G. Steinfeld, and M. KÜhn, "Field investigation on the influence of yaw misalignment on the propagation of wind turbine wakes," *Wind Energy*, vol. 21, no. 11, pp. 1011–1028, Nov. 2018.

[11] P. Mckay, R. Carriveau, and D. S.-K. Ting, "Wake impacts on downstream wind turbine performance and yaw alignment," *Wind Energy*, vol. 16, no. 2, pp. 221–234, Mar. 2013.

[12] T. F. Pedersen, S. Gjerding, and P. Ingham, "Wind turbine power performance verification in complex terrain and wind farms," Risø Nat. Lab., Roskilde, Denmark, Tech. Rep. Risø-R-1330, Apr. 2002.

[13] D. Schlipf, S. Kapp, J. Anger, O. Bischoff, M. Hofsäß, A. Rettenmeier, and M. Kühn, "Prospects of optimization of energy production by LIDAR assisted control of wind turbines," in *Proc. Ewea Annu. Event*, Brussels, Belgium, 2011, pp. 14–17.

LE ZHANG was born in Nanjing, Jiangsu, China, in 1980. He received the B.S., M.S., and Ph.D. degrees in electrical engineering from the Nanjing University of Aeronautics and Astronautics.

From 2009 to 2015, he was engaged in scientific research in government institutions. In 2016, he joined Wuxi Taihu University, where he became a Teacher. In 2019, he won the title of an Associate Professor. He has published 15 academic articles in journals and authorized eight national invention patents. He has obtained the support of many government and enterprise funds. His research interests involve wind power generation, motor control, industrial informatization, and other fields.

QIANG YANG (Senior Member, IEEE) received the B.S. degree (Hons.) in electrical engineering and the M.Sc. (Hons.) and Ph.D. degrees in electronic engineering and computer science from the Queen Mary College, University of London, London, U.K., in 2003 and 2007, respectively.

He visited the University of British Columbia and the University of Victoria Canada, as a Visiting Scholar, in 2015 and 2016, respectively. He is currently a Full Professor with Wuxi Taihu University, China. He has published more than 160 technical articles, applied 60 national patents, coauthored two books, and several book chapters. His research interests over the years include communication networks, smart energy systems, and large-scale complex network modeling, control, and optimization. He is a member of IET and IEICE and a Senior Member of the China Computer Federation (CCF).